Front. Chem. Sci. Eng. 2023, 17(12): 1962–1972
https://doi.org/10.1007/s11705-023-2359-z

RESEARCH ARTICLE

Enhanced activity of bimetallic Fe-Cu catalysts supported on ceria toward water gas shift reaction: synergistic effect

Gianluca Landi (✉)[1], Giulia Sorbino[1], Fortunato Migliardini[1], Giovanna Ruoppolo[1], Almerinda Di Benedetto[2]

1 Institute of Sciences and Technologies for Sustainable Energy and Mobility-CNR, Naples 80125, Italy
2 Department of Chemical, Materials and Production Engineering, University of Naples Federico II, Naples 80125, Italy

Abstract Within the "hydrogen chain", the high-temperature water gas shift reaction represents a key step to improve the H_2 yield and adjust the H_2/CO_x ratio to fit the constraints of downstream processes. Despite the commercial application of the high-temperature water gas shift, novel catalysts characterized by higher intrinsic activity (especially at low temperatures), good thermal stability, and no chromium content are needed. In this work, we propose bimetallic iron-copper catalysts supported on ceria, characterized by low active phase content (iron oxide + copper oxide < 5 wt %). Fresh and used samples were characterized by inductively coupled plasma mass spectrometry, X-ray diffraction, nitrogen physisorption, scanning electron microscopy coupled with energy-dispersive X-ray spectroscopy, and temperature programmed reduction in hydrogen to relate physico-chemical features and catalytic activity. The sample with iron/copper ≈ 1 and 4 wt % active phase content showed the best catalytic properties in terms of turnover frequency, no methane formation, and stability. Its unique properties were due to both strong iron-copper interaction and strong metal-support interaction, leading to outstanding redox behavior.

Keywords water gas shift, iron, copper, bimetallic catalysts, ceria, hydrogen

1 Introduction

Renewable hydrogen production has been considered in the last decades as a fundamental step toward the sustainability of energy production and H_2-related processes, such as in refineries and metallurgy [1]. In this context, the flexibility of hydrogen production from different sources represents a key feature for its employment as energy carrier in the transition from fossil to renewable sources. Hydrogen can be produced not only by direct conversion of electric power (photovoltaic, wind) through electrolysis but also by thermochemical conversion of fossil and renewable fuels, such as natural gas, biogas, biomasses, coke, and wastes [2,3]. The so-produced synthesis gas can be further upgraded by water gas shift (WGS) reaction (Eq. (1)) to improve the H_2 yield and adjust the H_2/CO_x ratio to fit the constraints of downstream processes (H_2 purification, CO_2 separation, Fisher-Tröpsch synthesis, methanol synthesis, methanation, etc.).

$$CO + H_2O \leftrightarrow CO_2 + H_2 \quad (1)$$

WGS is a mildly exothermic reaction (ΔH = –41.1 kJ·mol^{-1}), thermodynamically limited in a wide temperature range. Accordingly, WGS is generally carried out at different temperatures: low-temperature WGS (150–250 °C), medium-temperature WGS (MT-WGS, 250–320 °C), and high-temperature WGS (HT-WGS, 320–450 °C) [4]. At each temperature, different catalysts are used: copper-based catalysts are the most active at low temperatures [4], while iron-based catalysts are commonly used in HT-WGS [4]. Regarding the MT-WGS, the most interesting catalytic systems are based on noble metals, mainly Au and Pt [5–8]. HT-WGS is commercially catalyzed by iron-chromium mixed oxides. Recently, there has been a significant interest in the development of novel HT-WGS catalysts [4,9]. As reported by Baraj et al. [4], the main drawbacks of Fe-Cr-based catalysts are related to their poor activity at low temperatures, possible leaching of hexavalent chromium, and sintering (especially at lower Cr content). Accordingly, the main efforts have been devoted to the improvement of the intrinsic activity and/or the replacement of chromium. Doping with transition metals [10,11] has been investigated with promising results.

Received May 12, 2023; accepted July 25, 2023;
online October 13, 2023

E-mail: gianluca.landi@cnr.it

Copper addition resulted in improved performance due to an easier iron reduction [12]. Accordingly, the bimetallic Fe-Cu systems have been investigated, generally showing higher reaction rates than the corresponding iron catalysts toward both direct [10,13,14] and reverse [15] WGS reactions.

The elements selected to substitute chromium are mainly aluminum, magnesium, and cerium. They were added to bulk catalysts as "spacers" rather than as supports. Good results have been reported in terms of activity and stability by replacing Cr with Al, especially on bimetallic Fe-Cu systems [14,16]. The promising performance and stability can be ascribed to the higher surface area [17]. The good thermostability of Al-doped catalysts was addressed to the surface structure and the particle size similar to the undoped catalyst [18]. Similar results in terms of stability were obtained by adding Ce to iron-based catalysts [19,20].

Ceria is a well-known catalyst support for metals/metal oxides providing improved redox properties [21,22] due to the strong metal-support interaction (SMSI) [23] and electronic metal support interaction [24]. Cu-Ce systems, have been tested in low-temperature CO oxidation, showing that the highly surface-dispersed oxygen species related to the CuO_x are the active species [25]. In CO_2 hydrogenation, it has been shown that ceria plays the key role of activating CO_2, while CuO_x is crucial for H_2 activation [26]. In the case of Fe-Pt/Ce systems, it has been shown that the designed anchoring of Fe and Pt atoms on the CeO_2 surface can enhance the reverse WGS process [27], and this has shed light on the importance of creating dual sites to improve catalytic performance.

In this work, we propose bimetallic Fe-Cu catalysts supported on ceria as HT-WGS catalysts. The work aims at improving the performance of Cr-free catalysts at temperatures lower than 400 °C and testing the stability. Here proposed catalysts are characterized by low active phase content (Fe_2O_3 + CuO < 5 wt %), with respect to similar WGS catalysts (i.e., iron and copper oxides) [19,20]. Fresh and used samples were characterized by inductively coupled plasma mass spectrometry (ICP-MS), X-ray diffraction (XRD), N_2 physisorption, scanning electron microscopy coupled with energy-dispersive X-ray spectroscopy (SEM-EDS), and temperature programmed reduction in hydrogen (H_2-TPR) to relate physico-chemical features and catalytic activity. To better understand the key features of the proposed catalysts, samples with different Fe/Cu ratios and monometallic catalysts supported on ceria were prepared. In addition, a bimetallic catalyst supported on γ-alumina was prepared to study the role of ceria. The catalytic performances were tested and compared to those of the commercial catalyst.

Similar catalysts were recently tested in the reverse WGS reaction at high temperatures (up to 750 °C) to overcome thermodynamic limitations, and the redox properties were not characterized [28].

2 Experimental

2.1 Materials preparation

The supported catalysts were prepared by wet impregnation. Iron nitrate nonahydrate ($Fe(NO_3)_3{\cdot}9H_2O$) and copper nitrate hemi-pentahydrate ($Cu(NO_3)_2{\cdot}2.5H_2O$) were purchased from Sigma-Aldrich and used as received. Commercial ceria (Treibacher) and γ-alumina (CK-300) were used as supports. An aqueous solution was prepared by solving stoichiometric amounts of iron and/or copper nitrates in bi-distilled water. Impregnation was carried out by rotary evaporation (t = 60 °C, 120 r·min^{-1}, under vacuum at 20 kPa). Then, the samples were dried in a stove at 120 °C and were calcined in an oven at 550 °C for 2 h to decompose the nitrates.

A commercial catalyst (Clariant ShiftMax® 120 HCF) was also tested and used as reference. Table 1 shows the nominal compositions of the prepared samples as well as the label used thereof. All the samples are supported on ceria except FC-A, which is supported on γ-alumina. Generally, the active phase content was fixed at 4 wt %, while the Fe_2O_3/CuO weight ratio was changed between 0.2 (sample F5C) and 10 (sample 10FC). Sample 2(FC) is characterized by a Fe_2O_3/CuO weight ratio equal to 1 and an overall active phase content equal to 8 wt %.

2.2 Materials characterization

The composition was determined by employing ICP-MS analysis by an Agilent 7500CE instrument. Results (Table 1) showed differences with the nominal content within the experimental error (±10%).

XRD spectra were collected with an XRD diffractometer, PANalytical X'Pert Pro. The measurements were carried out with a step size of 0.02° and a counting time of 80 s per step.

Brunauer-Emmett-Teller (BET) SSA of fresh and used materials were measured by N_2 adsorption at 77 K with a Quantachrome Autosorb-1C instrument after degassing the samples at 150 °C for 1.5 h.

Catalyst morphology was observed using a FEI Inspect Scanning Electron Microscope equipped with an energy-

Table 1 Materials tested for the thermochemical splitting process

Sample	Fe_2O_3/(wt %)		CuO/(wt %)		Surface areas (SSA)/(m^2·g^{-1})
	Nominal	Measured	Nominal	Measured	
F	4.00	4.06	–	–	46.6
C	–	–	4.00	4.20	45.6
FC	2.00	2.02	2.00	1.83	54.3
10FC	3.64	3.80	0.36	0.49	53.2
5FC	3.33	3.30	0.67	0.73	48.6
F5C	0.67	0.72	3.33	3.60	51.1
2(FC)	4.00	3.81	4.00	4.15	47.0
FC-A	2.00	2.12	2.00	1.95	170.0

dispersive X-ray probe for the elemental analysis.

H_2-TPR was carried out by using a Micromeritics TPD/TPR 2900 analyzer, equipped with a thermal conductivity detector, operating with a 2% H_2/Ar mixture (25 $cm^3 \cdot min^{-1}$ flux) and a heating rate of 10 °C·min^{-1} from room temperature up to 550 °C. Samples were not pre-treated.

Reduction profiles were deconvoluted employing the OriginPro 8.5 software.

2.3 Catalytic tests

The experimental rig was described elsewhere [29]. The powder sample (600 mg; 200–400 μm) was placed in a tubular quartz reactor and inserted into an electric tubular furnace (Lenton). A thermocouple placed inside a tube co-axial with the reactor provided the measurement of the catalyst temperature. The gaseous feed and products were monitored with a Fisher-Rosemount NGA2000 continuous analyzer, equipped with an NDIR module measuring CH_4, CO, and CO_2 concentrations, a paramagnetic detector measuring O_2 concentration, and a thermal conductivity detector measuring H_2 concentration. Catalytic tests were run at fixed contact time, defined as the (catalyst weight)/(flow rate) ratio and equal to 0.108 g·s^{-1}·cm^{-3}. Reaction temperature ranged from 300 to 500 °C. Methane formation was not detected in any experimental tests, suggesting that the methanation reaction is not activated by the proposed catalysts. Mass balance was always closed within ± 5%. CO conversion was calculated according to the following equation:

$$x = \frac{CO_{in} - CO_{out}}{CO_{in}}. \quad (2)$$

Equilibrium calculations were carried out with Aspen Plus (AspenTech). Equilibrium was calculated by minimizing Gibbs free energy at specified operating conditions. Since methanation is not activated by the used catalysts, equilibrium was calculated by excluding methane from the products.

3 Results and discussion

3.1 Characterization of the materials

BET surface areas of fresh samples are reported in Table 1. Concerning about the corresponding supports (ceria: 55 $m^2 \cdot g^{-1}$; γ-alumina: 180 $m^2 \cdot g^{-1}$), the SSAs of the fresh catalysts are slightly lower as expected. SSA of used samples (not reported) are like those of the fresh ones. Samples before and after reaction were investigated via XRD analysis. The patterns of fresh (shown in Fig. 1) and used catalysts are very similar.

Each profile of ceria-supported samples shows typical peaks of fluorite structure with reflections at 2θ = 28.870°, 48.049°, 57.012°, as expected for CeO_2 systems. No diffraction peak due to copper and/or iron oxides was detected, suggesting good dispersion of the active phase onto the support surface. No significant modification of reflection angles was detected, suggesting negligible embedding of copper and/or iron into the fluorite structure, as previously reported [30,31]. On the contrary, the alumina-supported catalyst shows peaks attributable to phases different from the support. Peaks addressed to Fe_2O_3 (2θ = 60.58°) and to $CuFeO_2$ (2θ = 31.26°, 35.03°, 37.66°) are detected, suggesting a lower dispersion of the active phase despite the higher specific surface area of the support.

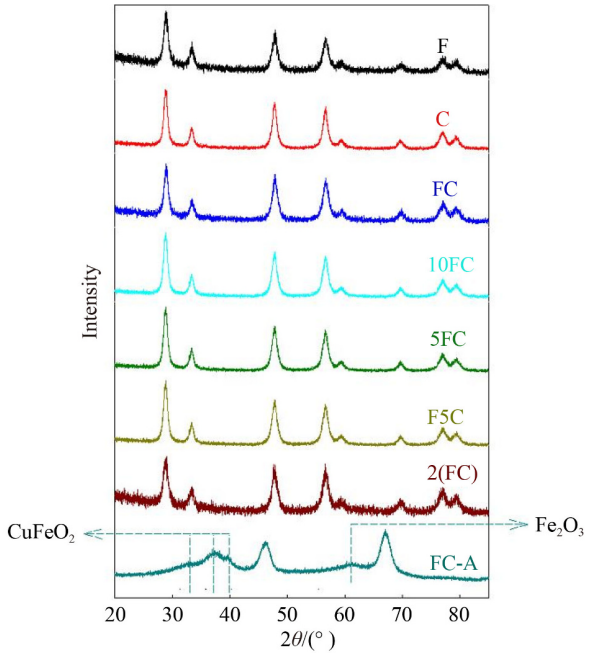

Fig. 1 XRD profiles of fresh samples.

Figure 2 shows the images of the samples and the corresponding elemental analysis, obtained by SEM-EDS analysis. In agreement with XRD results, all the samples show similar morphology and a quite homogeneous surface distribution of iron, copper, and cerium, confirming the good dispersion of the active phase onto the support. The results of the H_2-TPR tests carried out on iron-copper/ceria-based catalysts are shown in Fig. 3, in terms of hydrogen consumption and temperature as a function of time-on-stream. Ceria reduction starts at temperatures above 400 °C [32]. Small amounts of transition metals significantly modify the TPR profiles, which show two or three reduction peaks at temperatures lower than those of pure ceria [33–35]. It is worth noting that CuO reduction under similar heating rates occurs at about 300–350 °C [36], while the reduction of Fe_2O_3 to Fe_3O_4 and to metallic Fe occurs at about 500 and 700 °C, respectively [12,37].

As shown in Fig. 3, the catalysts supported on ceria (F samples excluded) start to be reduced at about 200 °C and

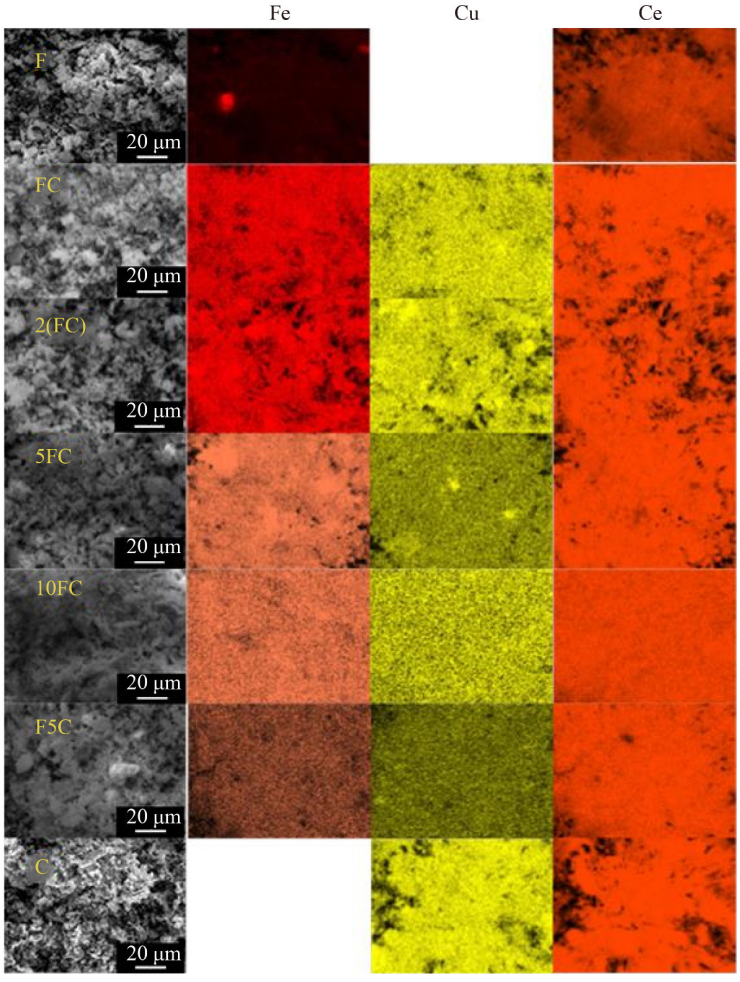

Fig. 2 SEM images (3000×) and corresponding EDS analyses of fresh samples.

show two or three reduction peaks. The fresh F sample shows a single reduction peak at about 400 °C. This peak can be attributed to iron reduction promoted by ceria and/or ceria reduction promoted by iron oxide [37,38]. The H_2-TPR profile of the used sample is practically unchanged. The fresh C sample shows a TPR profile similar to those of other copper/ceria catalysts [31,33,39], characterized by a peak at about 230 °C with a shoulder at about 200 °C. Equilibrating under reaction conditions causes a reduction of the overall H_2 consumption and separation of the main reduction peak into two overlapped peaks. According to the literature results, we found that in bimetallic iron-copper/ceria catalysts, copper-iron interaction significantly increases the reducibility with respect to the fresh catalysts [15,37]. A peak is detected at about 500 °C on iron-rich samples, corresponding to the reduction of iron oxide clusters. Accordingly, on increasing the copper content, this peak decreases, up to disappearing at Fe/Cu = 1. Interestingly, these clusters are reduced at temperatures typical of unsupported iron oxide, suggesting that they do not strongly interact with ceria, in agreement with the results by Kaihang Han et al. [40] showing that on Cu-Ni/Si catalysts, the interaction between Ni–Cu and SiO_2 is reduced with the increasing of the Cu load. As stated above, the overall reducibility of these catalysts improves on bimetallic samples. The main reduction occurs in two quite overlapped peaks below 300 °C. By doubling the active phase content, i.e., comparing FC and 2(FC), the high-temperature peak appears again, suggesting the formation of isolated iron oxide clusters. The significant role of ceria can be identified by comparing the H_2-TPR profiles of fresh FC and FC-A. On the alumina-supported sample, a lower H_2 consumption is found, at about 300 °C. The bimetallic interaction shifts the reduction at lower temperatures [16], and the strong interaction between Fe-Cu sites and ceria provides a synergistic effect. The reaction environment slightly changes the TPR profiles: a partial reduction is found as evidenced by the reduction of the areas of H_2 consumption.

Figure 4 and Table 2 show the quantitative results in terms of hydrogen consumption per gram of catalyst. Overall consumptions are reported in Table 2 as well as the ratios between the actual and theoretical H_2 consumptions (H_2/H_{2_t}). To calculate the theoretical H_2 uptakes, copper oxide as CuO was reduced to its metallic

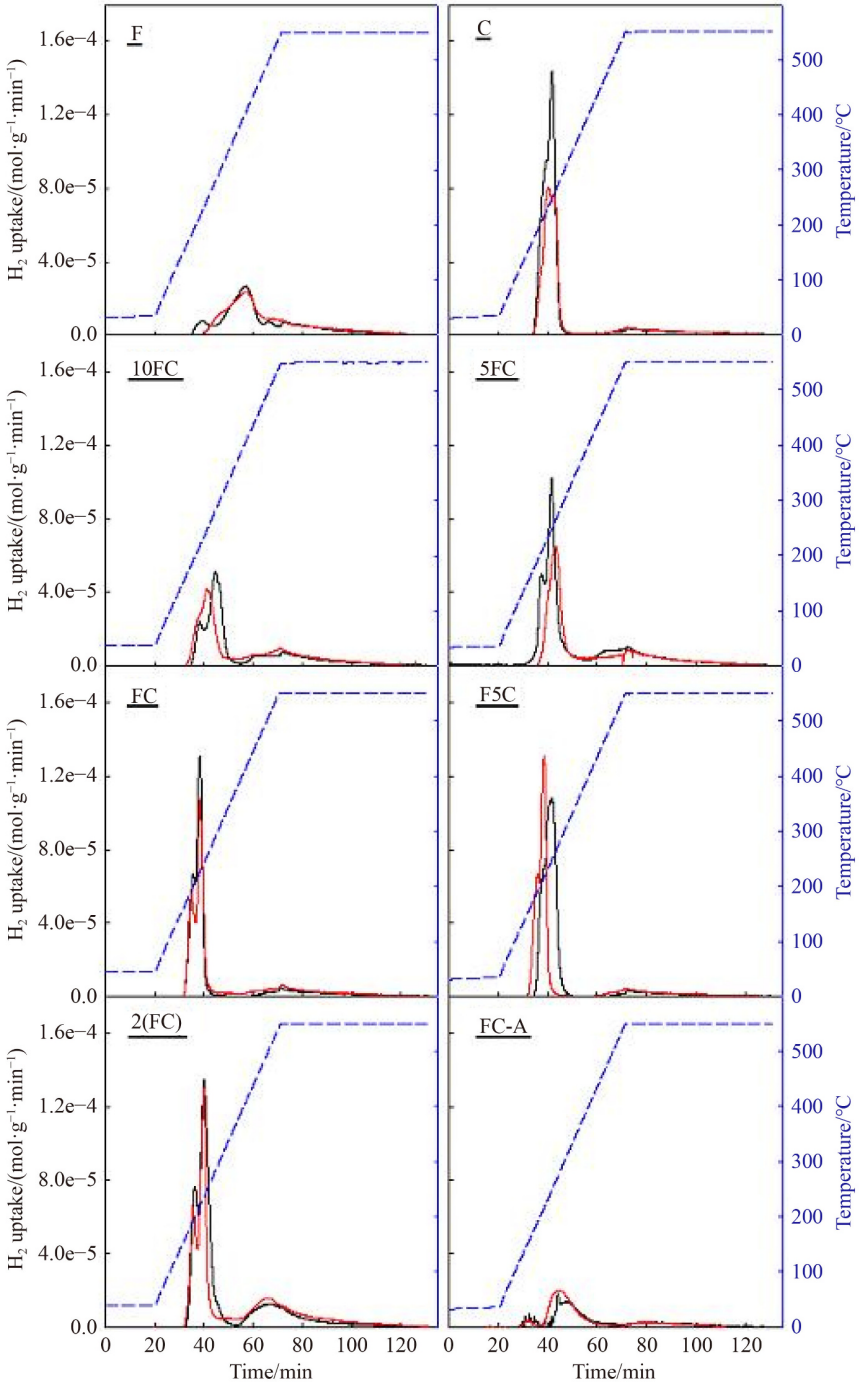

Fig. 3 H_2-TPR profiles of fresh (black continuous lines) and used (red continuous lines) catalysts; and temperature profiles (blue dashed lines).

state, while three different iron oxide reductions were considered: (1) Fe_2O_3 to Fe_3O_4 ($1\_H_2/H_{2\_t}$); (2) Fe_2O_3 to FeO ($2\_H_2/H_{2\_t}$); (3) Fe_2O_3 to Fe ($3\_H_2/H_{2\_t}$). TPR profiles were deconvoluted according to the procedure described in Section 2.2. The results of this procedure are reported in Fig. 4, showing the H_2 uptake as a function of the peak temperatures.

C sample shows an over-reduction, as suggested by the H_2 uptake higher than the theoretical one, due to the contribution of ceria to the reduction of interfacial Cu-Ce sites (Table 2) [34,39]. The reaction environment causes a slight re-organization, as evidenced by the detection of two better-defined peaks (Fig. 3). The F sample shows similar H_2 consumptions before and after the reaction, but with two different distributions. Accordingly, the reaction seems to promote iron re-allocation onto the ceria surface providing a more homogeneous site distribution. The $1\_H_2/H_{2\_t}$ ratio is higher than $3\_H_2/H_{2\_t}$, suggesting that

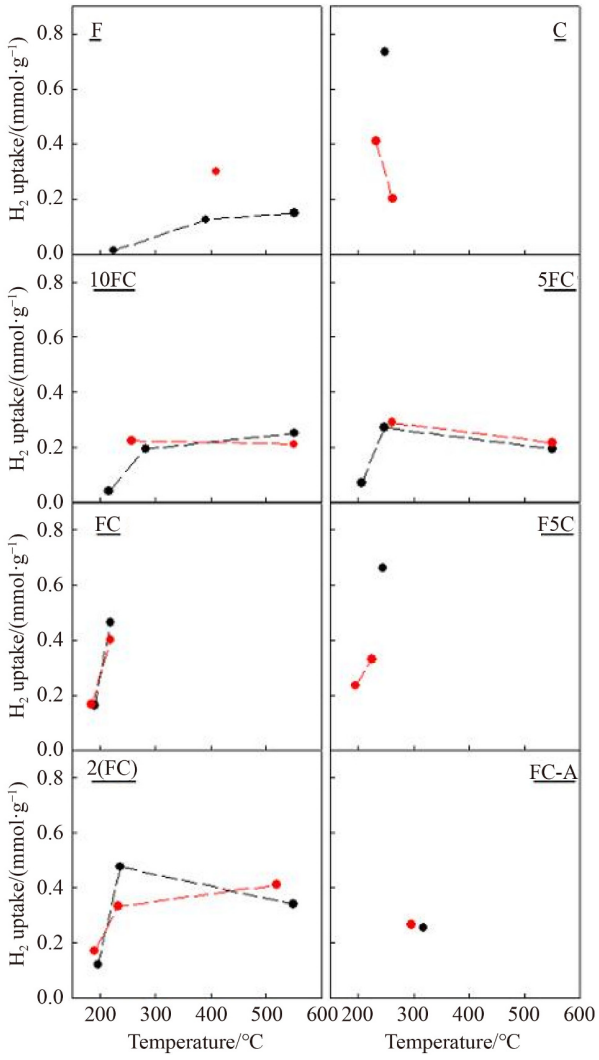

Fig. 4 H_2-TPR: H_2 consumption for different peaks as a function of peak temperature for fresh (black symbols) and used (red symbols) catalysts.

Table 2 H_2 uptakes and ratios between actual and theoretical H_2 consumptions for fresh and used catalysts

Sample	H_2 uptake/ (μmol·g^{-1})		H_2/H_{2_t} [(a)]		$2\_H_2/H_{2\_t}$ [(b)]		$3\_H_2/H_{2\_t}$ [(c)]	
	Fresh	Used	Fresh	Used	Fresh	Used	Fresh	Used
F	289	301	3.41	3.55	1.14	1.18	0.38	0.39
C	735	611	1.39	1.16	1.39	1.16	1.39	1.16
FC	627	567	2.38	2.15	1.80	1.63	1.04	0.94
10FC	484	435	3.56	3.20	1.64	1.48	0.63	0.56
5FC	535	505	2.96	2.79	1.68	1.59	0.73	0.69
F5C	661	566	1.41	1.21	1.31	1.13	1.10	0.94
2(FC)	936	911	1.56	1.52	1.23	1.20	0.76	0.74
FC-A	255	267	0.88	0.92	0.67	0.70	0.40	0.41

(a) Iron reduction: $Fe_2O_3 \rightarrow Fe_3O_4$; (b) iron reduction: $Fe_2O_3 \rightarrow FeO$; (c) iron reduction: $Fe_2O_3 \rightarrow Fe$; (a), (b), (c) copper reduction: $CuO \rightarrow Cu$

magnetite is not the final TPR product. On the other hand, the $2\_H_2/H_{2\_t}$ and $3\_H_2/H_{2\_t}$ ratios are higher and lower than 1 respectively. As reported above, iron reduction to its metallic state occurs at a temperature above 700 °C [12,37]; thus, we could speculate that iron is reduced to Fe^{2+} and the overall H_2 uptake is affected by partial ceria reduction as occurring for copper oxide. The comparable hydrogen uptakes for the fresh and used samples suggest that the metallic iron is not generated during the reaction, thus explaining the null activity toward the methanation reaction.

The behavior of the bimetallic FC catalyst is quite different from that of the monometallic samples. The two reduction peaks resemble those of the C sample; however, they are shifted at even lower temperatures. More interestingly, no re-organization occurs under reaction conditions, as evidenced in Fig. 4, showing that the number of the peaks and their characteristic temperature are unaltered. In this case the $2\_H_2/H_{2\_t}$ also appears the most convincing, suggesting that, on bi-metallic samples supported on ceria, the metals (Fe, Cu, Ce) interaction enable a facile reduction of Cu^{2+} and Fe^{3+} to Cu^{+} and Fe^{2+} [37]. This sample shows the highest $2\_H_2/H_{2\_t}$ (Table 2).

Iron-rich samples show H_2 uptake distributions with features of both the F and FC samples. Low-temperature reduction is related to bimetallic sites in contact with ceria, while high-temperature reduction seems related to excess iron oxide poorly interacting with the support. Used samples show a re-organization characterized by a reduction of the peak number, as occurring for the F sample (Fig. 4). Interestingly, iron-rich samples show similar $2\_H_2/H_{2\_t}$ values (Table 2), that are included among those of F and FC samples. The copper-rich sample show H_2 uptake distributions with features of both the C and FC samples. Peak splitting after the reaction is typical of copper catalyst, but on the F5C sample, the peak temperatures of the used samples are more similar to those of the FC sample rather than to the C sample (Fig. 4). Also, the $2\_H_2/H_{2\_t}$ ratio is similar to that of the C catalyst (Table 2).

Doubling the active phase content provides the formation of a number of bimetallic sites in strict contact with ceria quite unchanged, as suggested by the H_2 uptakes distribution reported in Fig. 4. Furthermore, a significant amount of less reducible species is detected, probably due to an inhomogeneous active phase distribution, which is not detectable by XRD and SEM-EDS. The FC-A reduction clearly shows the role of ceria on the bi-metallic catalysts. H_2 uptake significantly decreases on the alumina-supported sample and, at the same time, the reduction temperature increases. Thus, ceria interaction with Fe-Cu sites improves redox properties from both quantitative and qualitative point of view.

3.2 Catalytic tests

Catalytic tests were carried out at reagent concentrations

equal to 1 vol % CO and 3 vol % H_2O at a contact time equal to 0.108 $g \cdot s^{-1} \cdot cm^{-3}$ and in the temperature range of 300–500 °C. As reported in Section 2.3, methane formation is negligible, suggesting that selectivity toward WGS is 100%. Methanation is catalyzed by metallic iron [4], which is not produced under reaction conditions, according to H_2-TPR results reported in Section 3.1. The performance will be reported in terms of CO conversion as a function of temperature.

Figure 5 shows the catalytic performance of ceria-supported samples with different Fe/Cu ratios, including monometallic catalysts. C sample shows a significant conversion at low temperatures and a mild increase in the performance at increasing temperatures, which is typical of a low activation energy value, possibly related to adsorption as the limiting step. F sample shows a very low conversion at 300 °C, but, differently from the C sample, CO conversion significantly increases by increasing the reaction temperature, suggesting that the limiting reaction step is probably the surface chemical reaction (generally showing high activation energy). Anyway, in both cases, equilibrium conversion is not attained, at the investigated temperatures. All the bimetallic samples show improved performance with respect to the monometallic ones. The F5C catalyst shows a behavior similar to the copper catalyst but shifted at higher conversion values. Increasing the Fe/Cu ratio to 1 (FC sample) significantly enhances the WGS activity of the catalyst: 84% CO conversion is found at 300 °C and equilibrium conditions are attained at higher temperatures. A further increase of the Fe/Cu ratio causes a partial loss of the activity, as suggested by the behavior of 5FC and 10FC samples, reaching thermodynamic conditions at about 450 °C.

The above results suggest that bimetallic Fe-Cu sites show significantly higher catalytic properties than the single metals, due to a synergistic effect. As reported in the previous Section, Fe-Cu interaction significantly changes the reducibility of the catalyst, which appears the main reason for the modifications of the catalytic activity. The fast reduction-oxidation of the FC sample, shown by both the H_2-TPR features and the absence of significant modifications of the TPR profiles before and after the reaction, is the key feature explaining the high activity of this sample.

Figure 6 compares the catalytic performance of monometallic catalysts, bimetallic catalysts with Fe/Cu = 1 supported on ceria and γ-alumina, and the commercial sample (Clariant ShiftMax® 120HCF). The alumina-supported sample (FC-A) shows the lowest activity, with a maximum CO conversion equal to 30% at temperatures above 450 °C, while the corresponding ceria-supported catalyst approaches the equilibrium conversion at a lower temperature (350 °C). It is worth noting that the positive effect of ceria can be related to both a better dispersion of the active phase, as evidenced by the XRD analysis, and an improved reducibility, as evidenced by the H_2-TPR measurements. These results highlight the fundamental role of ceria in the formation of surface bimetallic sites by the co-impregnation method.

Figure 6 also shows that by doubling the active phase content (2(FC) sample) the catalytic activity remains unchanged in the whole temperature range, except at the lowest temperature where a very slight increase of the conversion of 2(FC) sample can be found. Considering the high conversion values, this does not necessarily imply a marginal increase in the reaction rate. It is also notable that the CO conversion of the ceria-supported bimetallic catalysts is significantly higher than the commercial catalyst, at a temperature lower than 400 °C. To quantify the differences in the intrinsic activity of the catalysts, the kinetic constant was calculated for each sample. To this end, the reaction rate has been assumed as linear with respect to CO concentration. This assumption is valid only at low conversion, and very limited reaction conditions. Thus, the considerations would be qualitative rather than quantitative. Accordingly, the conversion degree can be calculated as a function of kinetic constant (k) and contact time (τ) as follows:

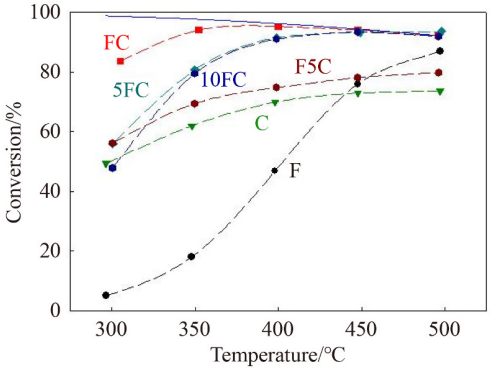

Fig. 5 CO conversion as a function of temperature, ceria-supported catalysts. Blue continuous line represents the equilibrium conversion.

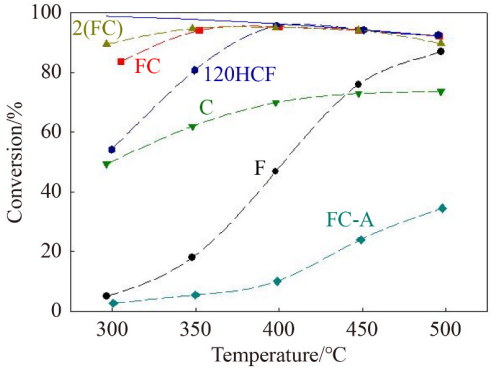

Fig. 6 CO conversion as a function of reaction temperature on monometallic, bimetallic catalysts with Fe/Cu = 1, and a commercial catalyst (120HCF). The blue continuous line represents the equilibrium conversion.

$$x = 1 - e^{-k\tau},$$

k values were calculated at 300 °C, where a difference between the actual conversion and the equilibrium conversion was measurable for all the samples.

In Fig. 7, the kinetic constant values are shown as a function of the Fe/(Fe + Cu) ratio. From a qualitative point of view, Fig. 7 shows a maximum for the Fe/Cu ratio of 1 (i.e., for Fe/(Fe + Cu) = 0.5), as expected. A fact less expected is the trend of the apparent kinetic constant in the right-hand section of the graph, i.e., for samples with Fe/Cu ⩾ 1. This trend suggests a linear dependence of the catalytic activity on the number of bimetallic sites Fe-Cu. This dependence is particularly evident because under these conditions the intrinsic activity of iron alone is much lower than the bimetallic sites. Conversely, at low values of Fe/(Fe + Cu) ratio (below 0.5), the trend is not linear, and the apparent kinetic constant results from a weighted average between the activity of the copper or iron sites and the activity of the bimetallic sites. Doubling the active phase content does not entail a doubling of the apparent kinetic constant, suggesting a lower efficacy in the use of the active phase on the sample with the greatest load, which is in agreement with the characterization results discussed in the previous section.

Table 3 summarizes the above results in terms of apparent turnover frequency (TOF), showing the highest intrinsic activity of the FC sample. Table 4 shows the performance of some of the most active catalysts reported in the scientific literature. The FC sample is one of the catalysts that show better performances. This finding not only provides evidence of the positive effect of the interaction among copper, iron, and ceria on the WGS activity but also suggests that FC catalyst could be an interesting alternative to commercial catalysts in industrial applications. The effect of feed composition was studied on the best catalyst, i.e., FC. Therefore, further catalytic tests were carried out at reactants concentrations equal to 0.5 vol % CO and 3.0 vol % H_2O and at reactants concentrations equal to 0.5 vol % CO and 1.5 vol % H_2O, to investigate the effect of the CO partial pressure at the same H_2O/CO ratio and the effect of the H_2O partial pressure at the same CO concentration. The same tests were carried out on F and C samples as reference.

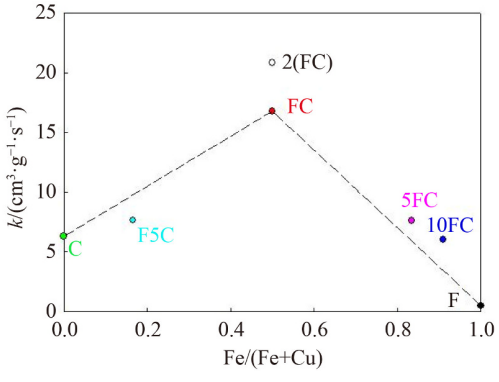

Fig. 7 Apparent kinetic constant calculated at 300 °C for ceria-supported samples as a function of the Fe/(Fe + Cu) ratio. Dashed lines represent the linear combination between i) the kinetic constant of the C sample and that of the FC sample for Fe/(Fe + Cu) < 0.5 and ii) the kinetic constant of FC samples and that of the F sample for Fe/(Fe + Cu) > 0.5.

Figure 8 shows the CO conversion as function of temperature for different feed compositions. On the F sample CO partial pressure negatively affects the reaction rate, while water vapor improves the kinetics. On the C sample at low temperatures, a slight positive effect of CO partial pressure and no effect of H_2O partial pressure is found, while at high temperatures the same conversion is found at H_2O/CO = 3, independently from the values of reactants concentrations. On increasing the H_2O/CO ratio, CO conversion increases, suggesting a change in the reaction mechanism between 400 and 450 °C. It is worth noting that the effects described above are not affected by thermodynamic constraints. FC catalyst shows completely different behavior. At low temperatures, on increasing the CO partial pressure, CO conversion increases, while an increase in H_2O partial pressure has a negative effect. At high temperatures, CO conversion reaches the equilibrium conversion. From these results, we may conclude that the reaction mechanism over the monometallic catalysts is significantly different from that over the bimetallic sample. The identification of these mechanisms is beyond the scope of this work.

All the tests were performed over the same sample which worked for more than 50 h. At the end of the

Table 3 Apparent TOF calculated at 300 °C for ceria-supported samples

Sample	TOF/(mol_{CO}·($mol_{(Fe+Cu)}$·s^{-1})$^{-1}$)
F	3.8×10^{-3}
C	5.1×10^{-2}
FC	1.4×10^{-1}
10FC	4.9×10^{-2}
5FC	6.2×10^{-2}
F5C	6.2×10^{-2}
2(FC)	8.5×10^{-2}

Table 4 Performance of catalysts reported in the literature and this work

Catalyst	Steam/carbon	τ/(g·s^{-1}·cm^{-3})	T/°C	Conv./%	Ref.
Cu-Ce	2.0	0.099	360	70	[41]
Fe-Cr-Cu	2.2	0.360	360	50	[13]
Fe-Al-Cu	1.0	0.060	400	65*	[16]
Fe-Ce-Co	3.5	0.126	500	50	[20]
Fe-Ni	4.5	0.700	400	75	[42]
FC	3.0	0.108	400	96*	This work

* Equilibrium conversion.

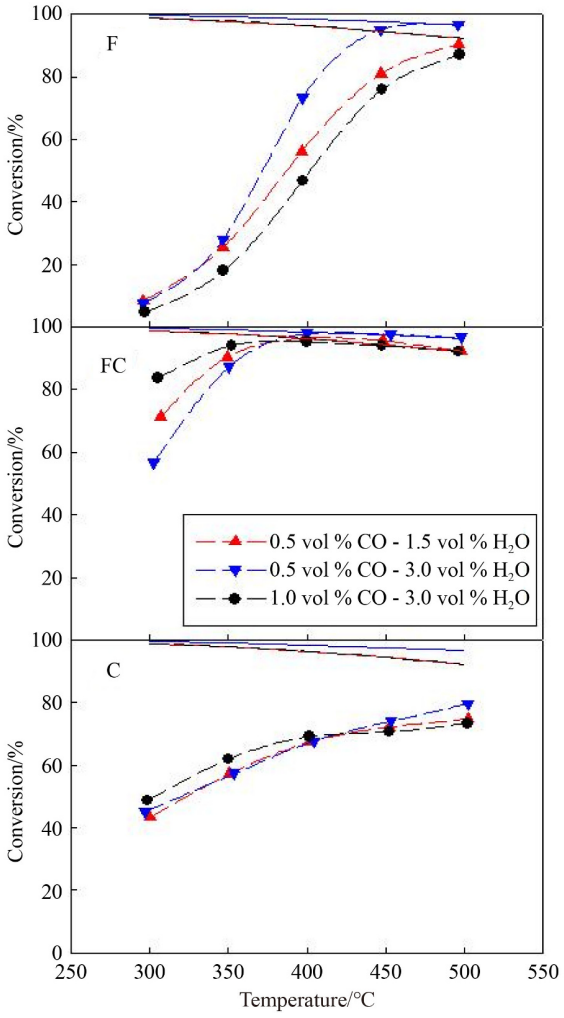

Fig. 8 CO conversion as a function of temperature, monometallic and bimetallic catalysts, Fe/Cu = 1 at different reactant concentrations. Continuous lines represent equilibrium conversions.

whole experimental campaign, catalytic tests were repeated to verify the catalyst stability. The results (not reported) were within the experimental error (±5%), suggesting good stability of the ceria-supported bimetallic Fe-Cu systems.

4 Conclusions

We successfully prepared bimetallic iron-copper catalysts supported on ceria by wet impregnation. The Cr-free catalysts were very active toward the HT-WGS reaction. In particular, the sample with Fe/Cu ≈ 1 and 4 wt % active phase content, showed the best catalytic performances in terms of turnover frequency, no methane formation, and stability. At relatively low temperatures, this catalyst outperformed all the tested samples, including the commercial Fe-Cr catalyst. These features are the result of concomitant factors: 1) homogeneous active phase distribution, leading to a strong Fe-Cu interaction; 2) an SMSI between the active phase and ceria. Due to the site interactions, the bimetallic Fe-Cu catalyst supported on ceria has shown an outstanding redox behavior as found by H_2-TPR. The sample is reduced at low temperature without forming metallic iron, explaining both the high intrinsic activity toward HT-WGS and the null activity toward methanation.

Preliminary tests at different reactant concentrations are promising and in future work the catalyst will be tested under applicative operative conditions.

Competing interests The authors declare that they have no competing interests.

Acknowledgements The authors gratefully acknowledge Mr. Andrea Bizzarro for BET analysis, Mr. Fernando Stanzione for ICP-MS measurements, and Mr. Luciano Cortese for XRD and SEM-EDS measurements. Open Access funding provided by Consiglio Nazionale Delle Ricerche within the CRUI-CARE Agreement.

References

1. Lee J E, Shafiq I, Hussain M, Lam S S, Rhee G H, Park Y K. A review on integrated thermochemical hydrogen production from water. International Journal of Hydrogen Energy, 2022, 47(7): 4346–4356
2. Hassan Q, Abdulateef A M, Hafedh S A, Al-samari A, Abdulateef J, Sameen A Z, Salman H M, Al-Jiboory A K, Wieteska S, Jaszczur M. Renewable energy-to-green hydrogen: a review of main resources routes, processes and evaluation. International Journal of Hydrogen Energy, 2023, 48(46): 17383–17408
3. Lee Y L, Kim K J, Hong G R, Roh H S. Target-oriented water-gas shift reactions with customized reaction conditions and catalysts. Chemical Engineering Journal, 2023, 458: 141422
4. Baraj E, Ciahotný K, Hlinčík T. The water gas shift reaction: catalysts and reaction mechanism. Fuel, 2021, 288: 119817
5. Cameron D, Holliday R, Thompson D. Gold's future role in fuel cell systems. Journal of Power Sources, 2003, 118(1–2): 298–303
6. de Oliveira C S, Teixeira Neto É, Mazali I O. Stabilization and Au sintering prevention promoted by ZnO in CeO_x-ZnO porous nanorods decorated with Au nanoparticles in the catalysis of the water-gas shift (WGS) reaction. Journal of Alloys and Compounds, 2022, 892: 162179

7. Li Y, Kottwitz M, Vincent J L, Enright M J, Liu Z, Zhang L, Huang J, Senanayake S D, Yang W C D, Crozier P A, Nuzzo R G, Frenkel A I. Dynamic structure of active sites in ceria-supported Pt catalysts for the water gas shift reaction. Nature Communications, 2021, 12(1): 914
8. Zhang Y, Jia A, Li Z, Yuan Z, Huang W. Titania-morphology-dependent Pt-TiO_2 interfacial catalysis in water-gas shift reaction. ACS Catalysis, 2023, 13(1): 392–399
9. Zhu M, Wachs I E. Iron-based catalysts for the high-temperature water-gas shift (HT-WGS) reaction: a review. ACS Catalysis, 2016, 6(2): 722–732
10. Rhodes C, Williams B P, King F, Hutchings G J. Promotion of Fe_3O_4/Cr_2O_3 high temperature water gas shift catalyst. Catalysis Communications, 2002, 3(8): 381–384
11. Lund C R F, Dumesic J A. Strong oxide-oxide interactions in silica-supported magnetite catalysts: IV. Catalytic consequences of the interaction in water-gas shift. Journal of Catalysis, 1982, 76(1): 93–100
12. Miccio F, Picarelli A, Ruoppolo G. Increasing tar and hydrocarbons conversion by catalysis in bubbling fluidized bed gasifiers. Fuel Processing Technology, 2016, 141: 31–37
13. Bahmani M, Nazari M, Mehreshtiagh M. A study on the mechanical strength of Fe_2O_3/Cr_2O_3/CuO catalyst for high temperature water gas shift reaction. Journal of Porous Materials, 2021, 28(3): 683–693
14. Zhang L, Wang X, Millet J M M, Matter P H, Ozkan U S. Investigation of highly active Fe-Al-Cu catalysts for water-gas shift reaction. Applied Catalysis A, General, 2008, 351(1): 1–8
15. Pastor-Pérez L, Baibars F, Le Sache E, Arellano-García H, Gu S, Reina T R. CO_2 valorisation via reverse water-gas shift reaction using advanced Cs doped Fe-Cu/Al_2O_3 catalysts. Journal of CO_2 Utilization, 2017, 21: 423–428
16. Zhang L, Millet J M M, Ozkan U S. Effect of Cu loading on the catalytic performance of Fe-Al-Cu for water-gas shift reaction. Applied Catalysis A, General, 2009, 357(1): 66–72
17. Popa T, Xu G, Barton T F, Argyle M D. High temperature water gas shift catalysts with alumina. Applied Catalysis A, General, 2010, 379(1–2): 15–23
18. Zhu M, Yalçın Ö, Wachs I E. Revealing structure-activity relationships in chromium free high temperature shift catalysts promoted by earth abundant elements. Applied Catalysis B: Environmental, 2018, 232: 205–212
19. Reddy G K, Smirniotis P G. Effect of copper as a dopant on the water gas shift activity of Fe/Ce and Fe/Cr modified ferrites. Catalysis Letters, 2011, 141(1): 27–32
20. Damma D, Boningari T, Smirniotis P G. High-temperature water-gas shift over Fe/Ce/Co spinel catalysts: study of the promotional effect of Ce and Co. Molecular Catalysis, 2018, 451: 20–32
21. Trovarelli A, Llorca J. Ceria catalysts at nanoscale: How do crystal shapes shape catalysis? ACS Catalysis, 2017, 7(7): 4716–4735
22. Aneggi E, Boaro M, Colussi S, de Leitenburg C, Trovarelli A. Ceria-based materials in catalysis: historical perspective and future trends. Handbook on the Physics and Chemistry of Rare Earths, 2016, 50: 209–242
23. Zhang J, Zhu D, Yan J, Wang C A. Strong metal-support interactions induced by an ultrafast laser. Nature Communications, 2021, 12(1): 6665
24. Chen J, Zhang Y, Zhang Z, Hou D, Bai F, Han Y, Zhang C, Zhang Y, Hu J. Metal-support interactions for heterogeneous catalysis: mechanisms, characterization techniques and applications. Journal of Materials Chemistry. A, Materials for Energy and Sustainability, 2023, 11(16): 8540–8572
25. Lu J, Wang J, Zou Q, He D, Zhang L, Xu Z, He S, Luo Y. Unravelling the nature of the active species as well as the doping effect over Cu/Ce-based catalyst for carbon monoxide preferential oxidation. ACS Catalysis, 2019, 9(3): 2177–2195
26. Xu J, Li L, Pan J, Cui W, Liang X, Yu Y, Liu B, Wang X, Song S, Zhang H. Boosting the catalytic performance of CuO_x in CO_2 hydrogenation by incorporating CeO_2 promoters. Advanced Sustainable Systems, 2022, 6(8): 2200287
27. Wang H, Bootharaju M S, Kim J H, Wang Y, Wang K, Zhao M, Zhang R, Xu J, Hyeon T, Wang X, Song S, Zhang H. Synergistic interactions of neighboring platinum and iron atoms enhance reverse water-gas shift reaction performance. Journal of the American Chemical Society, 2023, 145(4): 2264–2270
28. Chen L, Wu D, Wang C, Ji M, Wu Z. Study on Cu-Fe/CeO_2 bimetallic catalyst for reverse water gas shift reaction. Journal of Environmental Chemical Engineering, 2021, 9(3): 105183
29. Luciani G, Landi G, Aronne A, Di Benedetto A. Partial substitution of B cation in $La_{0.6}Sr_{0.4}MnO_3$ perovskites: a promising strategy to improve the redox properties useful for solar thermochemical water and carbon dioxide splitting. Solar Energy, 2018, 171: 1–7
30. Aneggi E, de Leitenburg C, Dolcetti G, Trovarelli A. Promotional effect of rare earths and transition metals in the combustion of diesel soot over CeO_2 and CeO_2-ZrO_2. Catalysis Today, 2006, 114(1): 40–47
31. Barbato P S, Colussi S, Di Benedetto A, Landi G, Lisi L, Llorca J, Trovarelli A. CO preferential oxidation under H_2-rich streams on copper oxide supported on Fe promoted CeO_2. Applied Catalysis A, General, 2015, 506: 268–277
32. Scirè S, Crisafulli C, Riccobene P M, Patanè G, Pistone A. Selective oxidation of CO in H_2-rich stream over Au/CeO_2 and Cu/CeO_2 catalysts: an insight on the effect of preparation method and catalyst pretreatment. Applied Catalysis A, General, 2012, 417–418: 66–75
33. Di Benedetto A, Landi G, Lisi L. Improved CO-PROX performance of CuO/CeO catalysts by using nanometric ceria as support. Catalysts, 2018, 8(5): 209
34. Di Benedetto A, Landi G, Lisi L. Nanostructured Catalysts for Environmental Applications. Cham: Springer, 2021, 79–112
35. Ronda-Lloret M, Rico-Francés S, Sepúlveda-Escribano A, Ramos-Fernandez E V. CuO_x/CeO_2 catalyst derived from metal organic framework for reverse water-gas shift reaction. Applied Catalysis A, General, 2018, 562: 28–36
36. Fedorov A V, Kukushkin R G, Yeletsky P M, Bulavchenko O A, Chesalov Y A, Yakovlev V A. Temperature-programmed reduction of model CuO, NiO and mixed CuO-NiO catalysts with hydrogen. Journal of Alloys and Compounds, 2020, 844: 156135
37. Yang L, Pastor-Pérez L, Villora-Pico J J, Sepúlveda-Escribano A, Tian F, Zhu M, Han Y F, Reina T R. Highly active and selective

multicomponent Fe-Cu/CeO_2-Al_2O_3 catalysts for CO_2 upgrading via RWGS: impact of Fe/Cu ratio. ACS Sustainable Chemistry & Engineering, 2021, 9(36): 12155–12166

38. Reina T R, Ivanova S, Domínguez M I, Centeno M A, Odriozola J A. Sub-ambient CO oxidation over Au/MOx/CeO_2-Al_2O_3 (M = Zn or Fe). Applied Catalysis A, General, 2012, 419–420: 58–66
39. Barbato P S, Colussi S, Di Benedetto A, Landi G, Lisi L, Llorca J, Trovarelli A. Origin of high activity and selectivity of CuO/CeO_2 catalysts prepared by solution combustion synthesis in CO-PROX reaction. Journal of Physical Chemistry C, 2016, 120(24): 13039–13048
40. Han K, Wang S, Hu N, Shi W, Wang F. Alloying Ni-Cu nanoparticles encapsulated in SiO_2 nanospheres for synergistic catalysts in CO_2 reforming with methane reaction. ACS Applied Materials & Interfaces, 2022, 14(20): 23487–23495
41. Lee Y H, Kim H M, Jeong C H, Jeong D W. Effects of precipitants on the catalytic performance of Cu/CeO_2 catalysts for the water-gas shift reaction. Catalysis Science & Technology, 2021, 11(19): 6380–6389
42. Park Y M, Cho J M, Han G Y, Bae J W. Roles of highly ordered mesoporous structures of Fe-Ni bimetal oxides for an enhanced high-temperature water-gas shift reaction activity. Catalysis Science & Technology, 2021, 11(9): 3251–3260